The EMBO Journal Vol.18 No.3 pp.543–554, 1999

The structure and function of a foot-and-mouth disease virus–oligosaccharide receptor complex

Elizabeth E.Fry[1], Susan M.Lea[1], Terry Jackson[2], John W.I.Newman[2], Fiona M.Ellard[2], Wendy E.Blakemore[2], Robin Abu-Ghazaleh[2], Alan Samuel[2], Andrew M.Q.King[2] and David I.Stuart[1,3,4]

[1]The Laboratory of Molecular Biophysics, Rex Richards Building, South Parks Road, Oxford OX1 3QU, [2]AFRC Institute for Animal Health, Ash Road, Pirbright, Woking GU24 0NF and [3]The Oxford Centre for Molecular Sciences, New Chemistry, South Parks Road, Oxford OX1 3QT, UK

[4]Corresponding author
e-mail: dave@biop.ox.ac.uk

Heparan sulfate has an important role in cell entry by foot-and-mouth disease virus (FMDV). We find that subtype O_1 FMDV binds this glycosaminoglycan with a high affinity by immobilizing a specific highly abundant motif of sulfated sugars. The binding site is a shallow depression on the virion surface, located at the junction of the three major capsid proteins, VP1, VP2 and VP3. Two pre-formed sulfate-binding sites control receptor specificity. Residue 56 of VP3, an arginine in this virus, is critical to this recognition, forming a key component of both sites. This residue is a histidine in field isolates of the virus, switching to an arginine in adaptation to tissue culture, forming the high affinity heparan sulfate-binding site. We postulate that this site is a conserved feature of FMDVs, such that in the infected animal there is a biological advantage to low affinity, or more selective, interactions with glycosaminoglycan receptors.

Keywords: heparan sulfate/protein–carbohydrate interactions/virus–receptor interactions/virus structure/X-ray crystallography

Introduction

Animal viruses infect host cells by the recognition of specific receptor molecules on the cell surface, followed by internalization and the transfer of viral nucleic acid, or nucleoprotein core, to the cytosol. These processes are important determinants of tissue tropism and key points where natural selection operates, yet despite intensive studies, the underlying molecular mechanisms remain largely obscure in terms of detailed structural descriptions. The small, icosahedral picornaviruses are particularly well studied both functionally and structurally (Rueckert, 1996); little is known of the structural details of how they recognize their receptors, with the exception of a low resolution cryo-electron microscopic (EM) reconstruction of a human rhinovirus associated with a soluble fragment of its intercellular cell adhesion molecule-1 (ICAM-1) receptor (Olson *et al*., 1993).

Foot-and-mouth disease virus (FMDV) causes a highly infectious disease in cloven-hooved animals, which can be economically devastating. It exists in seven serotypes (O, A, C, Asia, SAT1, SAT2 and SAT3), and has the basic picornavirus structure depicted in Figure 1 (terms defined there will be used throughout this paper). FMDV enters cells through receptor-mediated endocytosis followed by acid pH-dependent release and translocation of RNA across the endosomal membrane (Carrillo *et al*., 1984; Mason *et al*., 1994; Curry *et al*., 1995). FMDV can attach to cells via argine–glycine–aspartic acid (RGD)-binding integrin molecules (Surovoi *et al*., 1988; Fox *et al*., 1989; Baxt and Becker, 1990; Mason *et al*., 1994; Berinstein *et al*., 1995), such as $\alpha_v\beta_3$ (Berinstein *et al*., 1995; Jackson *et al*., 1997; Neff *et al*., 1998). The RGD tripeptide motif that recognizes the integrin is located in a long, flexible loop on the surface of the virion (Logan *et al*., 1993), and is found on all seven serotypes. Whilst mutations in this RGD motif are usually lethal (Mason *et al*., 1994) [except for viruses repeatedly passaged in tissue culture (Martinez *et al*., 1997)], competition studies (Sekiguchi *et al*., 1982) suggested that serotypes O and A use more than one receptor for cell attachment. This was clarified by the demonstration that for certain strains of O_1 FMDV, the predominant cell surface ligand is heparan sulfate (HS) (Jackson *et al*., 1996), and that attachment is both highly specific and necessary for efficient infection.

Sulfated glycosaminoglycans (GAGs), such as HS, are increasingly implicated in cell adhesion, in line with their ubiquitous distribution on cell surfaces as the carbohydrate component of proteoglycans (Salmivirta *et al*., 1996). These polymers of disaccharide repeats are highly sulfated. The basic repeating unit of heparin is L-iduronic acid (Idu) and D-glucosamine (GlcN) joined by an $\alpha(1–4)$ linkage (Figure 1). HS has a complex heterogeneous structure, which provides the potential for discriminating between different cell types through specific protein–sugar interactions. These properties of HS, and the observation that FMDV O_1BFS binds HS without the mediation of any other cellular component, led to the suggestion that infection might be initiated by two-step attachment, initial contact being with a low affinity HS proteoglycan receptor, followed by transfer to the high affinity integrin receptor for endocytosis (Jackson *et al*., 1996). A growing list of viruses use distinct receptors for attachment and internalization, including adenovirus type 2 (Wickham *et al*., 1993), several herpesviruses (WuDunn and Spear, 1989; Mettenleiter *et al*., 1990; Compton *et al*., 1993) and human immunodeficiency virus type 1 (HIV-1) (Feng *et al*., 1996; Clapham and Weiss, 1997; Wagner *et al*., 1998).

To understand how HS facilitates cell entry by FMDV, we have undertaken a quantitative study of the way cellular HS binds FMDV and enhances infection, together with a structural analysis of the receptor–virus complex.

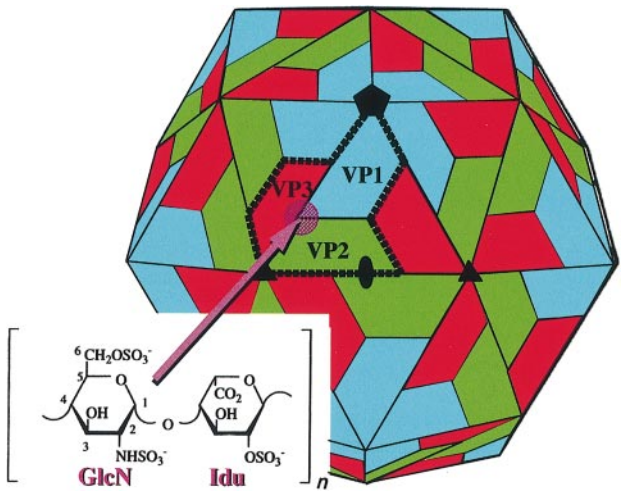

Fig. 1. A schematic depiction of the icosahedral capsid (symmetry axes labelled) which comprises 60 copies each of four virus-encoded proteins, VP1–VP4, with VP1–3 contributing to the external features of the capsid. These proteins are colour coded using a standard convention, which we use throughout the paper: VP1, blue; VP2, green; and VP3, red. A biological protomer, deriving from the uncleaved polyprotein, is defined in bold outline. Central to this subunit is the heparin-binding site. The inset shows a typical heparin disaccharide containing a total of three sulfate groups: one attached to the 2-hydroxyl group of Idu and two linked to the 2-amino and 6-hydroxyl groups of GlcN. In the non-bound structure, successive disaccharides within heparin are related by a 2-fold screw operation generated by a rotation angle of ~180° coupled to a translation of 8.0–8.7 Å along the helix axis.

We here report high resolution crystallographic analyses for FMDV O_1BFS complexed with various heparin and HS preparations. We have also extended the study to field isolates of FMDV, strain O_1Kaufbeuren (O_1K), closely related to O_1BFS. We find that the change of a single residue has profound biological consequences, effected through modulation of HS interactions.

Results

Receptor activity of HS

Measurements of the receptor activity of cell surface HS were made with two closely related FMDV strains O_1BFS and O_1KB64, both of which previously have been shown to depend on HS for their ability to produce plaques in cell monolayers (Abu-Ghazaleh, 1996). To quantify this dependence, an infectious centre assay was used to compare productive infectious events in wild-type CHO cells and the derivative cell line, psgD-677, which specifically lacks HS (Esko *et al.*, 1987). We previously have reported that the inability of psgD-677 cells to support plaque formation is caused by a defect in virus uptake, rather than in replication, and that this defect is directly attributable to the absence of HS rather than to any reduction in the expression of integrin receptors (Jackson *et al.*, 1996). By assaying infectious centres, we can see from Figure 2 that the HS-deficient cells are infectable by FMDV, but at a rate ~100-fold lower than that of their HS-bearing progenitors. The mechanism of the residual infectivity is unknown.

HS-binding sites could not be quantified on live CHO or MDBK cells, as the Scatchard plots were anomalous (data not shown). On paraformaldehyde-fixed MDBK

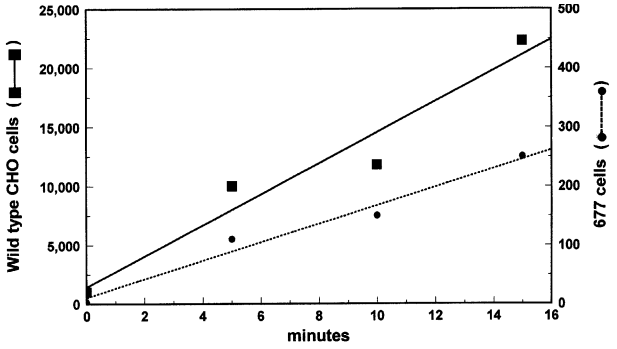

Fig. 2. Effect of cell surface HS on susceptibility to infection with O_1BFS. The numbers of productive infection events at 37°C were scored at the times indicated on wild-type CHO cells (solid line) or mutant (pgsD-677) cells lacking HS (dotted line), using the infectious centre assay described in Materials and methods. Different ordinate scales are used, one for the high number of infections (left side) and the other for the low number of infections (right side).

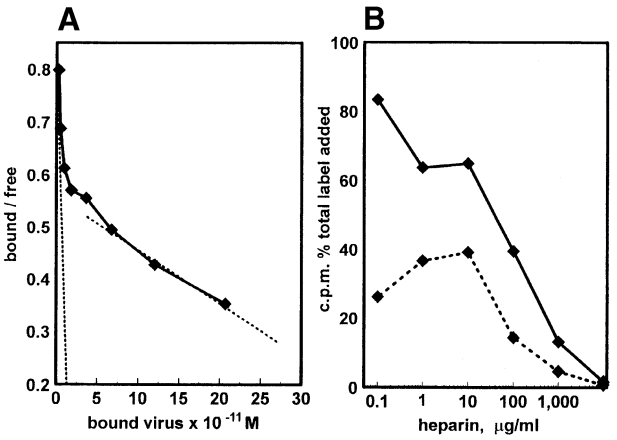

Fig. 3. Affinity of O_1KB64 FMDV for HS. (**A**) Scatchard analysis of virus (1100 c.p.m./ng) binding to fixed MDBK cells (4.0×10^4 cells/well; data in triplicate). (**B**) Inhibition of binding of radiolabelled virus to live BHK cells by heparin in the presence (dotted line) and absence (solid line) of a 100-fold excess of unlabelled virus. Virus samples were pre-equilibrated with the indicated amounts of bovine heparin in BBB for 30 min at 4°C. Data are means of quadruplicates. For binding studies with live cells (B), the virus was allowed to equilibrate with cells at 4°C for 10 h.

cells, however, the receptors could be resolved reproducibly into two distinct components (Figure 3A), a minor one (~5×10^3 sites/cell) having an apparent K_d of ~2×10^{-11} M, and a major component present at ~0.5×10^6 copies per cell, apparent K_d ~10^{-9} M. As the overwhelming majority of virus binding by MDBK cells is mediated through HS (Jackson *et al.*, 1996), the major component of the FMDV receptor population can be attributed to HS.

This confirms that HS is an abundant high-affinity ligand for FMDV O_1BFS on fixed cells. The affinity of HS on live cells, while not directly measurable, is likely to be higher still. A clue to just how much higher can be gained by comparing fixed and live cells for susceptibility of virus binding to competition by heparin. We have reported previously that heparin competes with HS on fixed cells at extremely low concentrations, with an IC_{50} in the range of 10–100 ng/ml for all cell types tested, including BHK-21, MDBK and CHO (Jackson *et al.*, 1996; data not shown). Figure 3B shows that, with live

Table I. Data processing

	O_1BFS/6 kDa heparin	O_1BFS/PEG/ 6 kDa heparin	O_1BFS/DTT/ 6 kDa heparin	O_1BFS/3 kDa heparin	O_1BFS/HS	O_1K/6 kDa heparin
Data processing						
No. of images	101	17	51	23	30	38
Total reflections	2 070 213	264 237	352 078	225 892	236 816	545 019
Independent reflections	480 875	117 171	232 267	156 187	148 495	145 735
Completeness (%)[a]	90.9 (77.4)	56.5 (53.0)	72.7 (34.2)	67.0 (27.0)	67.3 (56.0)	83.1 (60.1)
R_{merge} (%)[b]	14.3	11.0	8.8	12.4	10.8	11.6
MFID (%)[c]	8.1 (2.7 Å)	14.7 (2.7 Å)	10.6 (2.7 Å)	11.8 (2.7 Å)	11.0 (2.7 Å)	10.3 (2.8 Å)
dmin (Å)	1.9	2.6	2.25	2.5	2.55	2.75

[a]The figure in parentheses is for the highest resolution shell.
[b]$R_{merge} = [\Sigma\Sigma_{h\,i} |(<I_h> - I_{hi})|/(\Sigma\Sigma_{h\,i} I_{hi}] \times 100$, where h are unique reflection indices, I_{hi} are intensities of symmetry-redundant reflections and $<I_h>$is the mean intensity.
[c]MFID is the mean fractional isomorphous difference in structure factor amplitudes, compared with data from crystals of the native virus.

cells by contrast, ~10^3- to 10^4-fold more heparin is required for 50% inhibition of virus binding, implying that the affinity of live cell HS for FMDV exceeds that of fixed cell HS by a comparable number of orders of magnitude. Competition was studied at both low and high virus/cell multiplicities, the latter to eliminate complications due to the presence of small numbers of high affinity integrins. The main difference between the two plots of Figure 3B is not, however, in IC_{50}, which is relatively insensitive to the number of virus particles per cell, but in the enhancement in binding at intermediate heparin concentrations, presumably due to virus clumping; a smaller 'kink' was also seen reproducibly in the high specific activity virus plot at the same heparin concentration.

Crystallographic analyses of O_1BFS–HS receptor complexes

We have determined the structures of complexes of FMDV O_1BFS with HS by analyses of crystals of the virus soaked with each of two different molecular weight species of porcine heparin (approximate mean mol. wts 6 and 3 kDa) and with porcine HS. Data were collected at either 10 or 20 mg/ml concentration of sulfated oligosaccharide. Table I contains a summary of the various data sets collected. The centred lattice of the O_1BFS crystals accommodates ~30% solvent within channels of minimum diameter 50 Å, ample to permit diffusion of a 6 kDa sugar (a linear chain of ~10 disaccharide units). Data were collected to 1.9 Å (6 kDa soaked crystals) and 2.5 Å (3 kDa and HS soaked crystals). Difference maps calculated against the native O_1BFS data [$F_{o(soak)} - F_{o(native)}$] showed clear electron density for three saccharide units and weaker density corresponding to a further saccharide at either end. The electron density was rather blurred, suggesting either mobility or conformational heterogeneity for the bound oligosaccharide. An additional feature of these unbiased maps was the improved order of the VP1 C-termini beyond the point of interaction with the sugars at residue His195. Difference maps calculated between the various sets of heparin and HS soaked data [$F_{o(soakA)} - F_{o(soakB)}$] were essentially featureless, indicating that a common set of sulfated sugars was bound in similarly occupied conformations. Further heparin complexes were analysed for crystals soaked under differing conditions. Firstly the crystal mother liquor (~18% ammonium sulfate) was exchanged for PEG, to avoid solvent competition for sulfate-binding sites; the structure of the heparin–FMDV complex was unaffected. Incorporating dithiothreitol (DTT) into the soak to break the disulfide bond which normally disorders the integrin-binding VP1 G–H loop (Parry *et al*., 1990; Logan *et al*., 1993) led to a structure showing the G–H loop in the expected position, demonstrating that sugar binding does not perturb the conformation of the integrin-binding loop in either conformational state. Conversely, ordering of the loop had no effect on sugar binding.

The 6 kDa heparin data set extending to Bragg spacings of 1.9 Å was used as the basis for determining the structure of the complex. We modelled (Jones, 1985) and refined (Brünger, 1992) two sugar conformations starting from X-ray coordinates for heparin (courtesy of D.Rees; Faham *et al*., 1996). In the absence of convincing evidence for deviations from non-crystallographic symmetry (NCS), we maintained strict NCS constraints throughout the structure determination process. The final *R*-factor is 16.2%, with r.m.s.d. (bonds) of 0.014 Å. The electron density for the sugar remained blurred compared with the protein electron density, and in places there was convincing evidence for two principal conformations of bound sugar. A heparin model consisting of two pentasaccharides (CONF1 and CONF2) bound simultaneously at half occupancy satisfactorily explained most of the features of the electron density map (Figure 4A).

The conformation of the heparin receptor

Despite the heterogeneity in the HS and the range of different experiments performed, the electron density maps clearly show that the O_1BFS virus recognizes the same motif of sugars in each case The virus selects a fully sulfated heparin motif (Figure 1) as does basic fibroblast growth factor (bFGF) (Faham *et al*., 1996). The oligosaccharide has a relatively extended conformation, forming a banana-like structure which projects the outer disordered sugars away from the protein. The GlcN-2, Idu-3 and GlcN-4 rings constitute the three central residues, with poorly defined electron density for an additional sugar ring at either end (Figure 4A). The GlcN sugar rings and one of the terminal Idu rings adopt the energetically

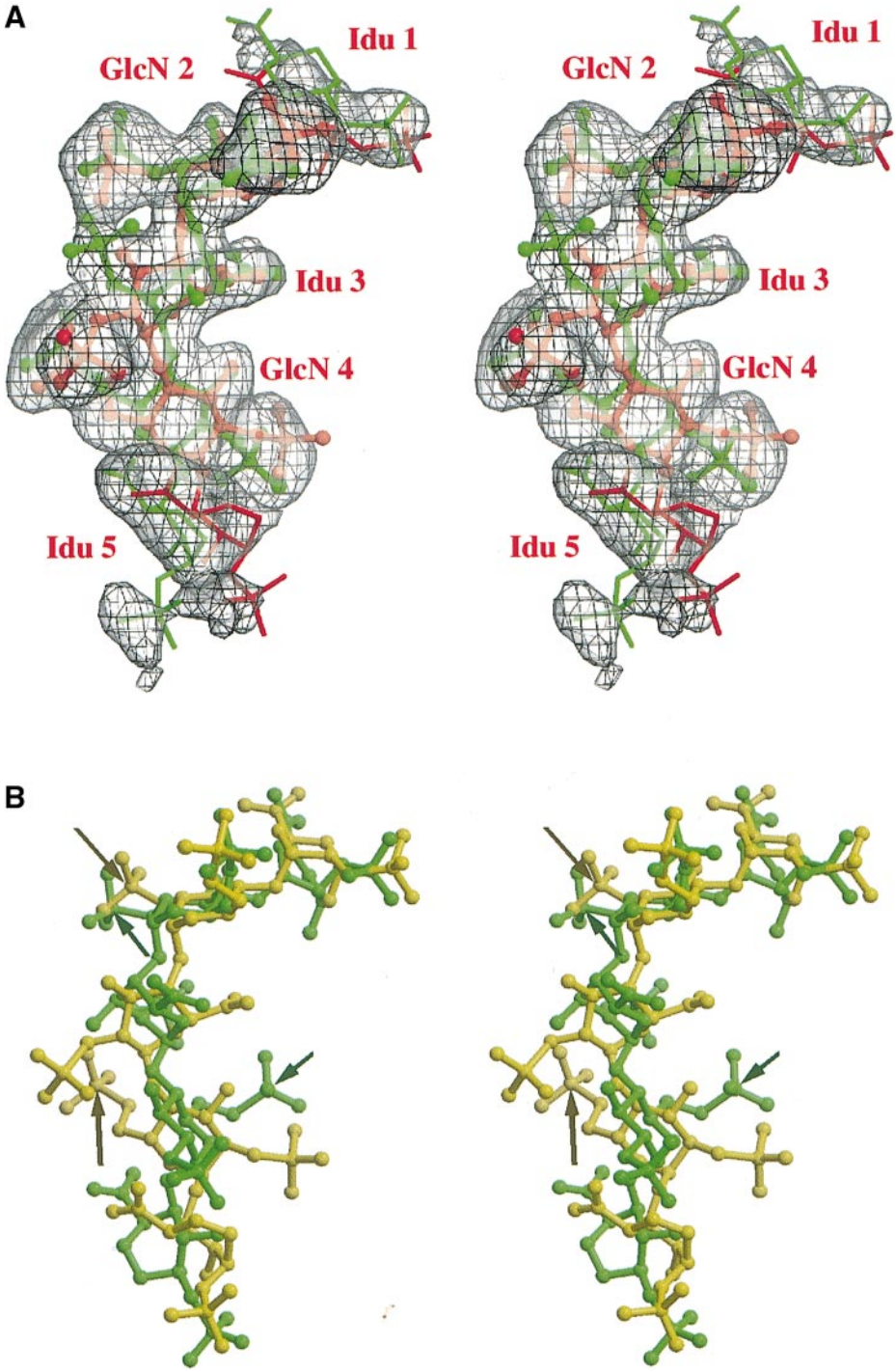

Fig. 4. (**A**) A Bobscript (Esnouf, 1997) and RASTER3D (Merritt and Murphy, 1994) stereo depiction of the 1.9 Å ($F_{obs} - F_{calc}$, $\alpha_{averaged}$) omit electron density map. Calculated structure factor amplitudes were generated from a model lacking heparin and the phases were derived from cyclic averaging (the starting phases for which were calculated from the same heparin minus model). The two heparin conformations are drawn, orientated with the sugars running from Idu-1 at the top to Idu-5 at the bottom, as ball-and-stick (CONF1, red and CONF2 green), with the outer sugars (Idu-1 and Idu-5) shown thinner commensurate with their lower accuracy. In CONF1, the oligosaccharide is stabilized by six internal hydrogen bonds, four via water molecules, and in CONF2 by eight internal hydrogen bonds, six via water molecules. (**B**) Stereo superimposition with bFGF. Coordinates for five sugar rings (CONF1) are shown in yellow using Bobscript (Esnouf, 1997) and RASTER3D (Merritt and Murphy, 1994) with a similar motif of sugars from the bFGF–heparin complex (Faham *et al*., 1996) (in green) having been superimposed using SHP (Stuart *et al*., 1979) only equivalencing the atoms that are reasonably similar. The orientation of the sugar chain is the same as in (A). The key sulfates that interact with Arg56 of VP3 are pinpointed along with the equivalent sulfates in the bFGF coordinates.

favourable $^4C_1$ or $^1C_4$ chair conformations (the other terminal Idu ring appears to adopt a $^{2,5}B$ conformation). The central Idu ring is seen in a skew boat $^2S_0$ conformation (CONF1) and also a $^1C_4$ chair conformation (CONF2) with the sulfate rotating about the C2–O2 bond by some 120° between these conformations, becoming adjacent to GlcN-2 in CONF2. The mobility of the sugar is facilitated by the flexibility of this Idu ring [Idu rings are generally

assumed to be more flexible than the GlcN rings (Casu *et al*., 1988; Forster and Mulloy, 1993)]. The GlcN and Idu sugar rings on either side apparently adopt a single conformation. The *B*-factors for the heparin motif are mostly lower in CONF1 than in CONF2 (average *B*-factors for the central Idu ring of 60 and 110 Å^2, respectively).

We find that the two more constrained rings, GlcN-2 and GlcN-4, provide key points of attachment to the virus. Flexibility at either end of the trisaccharide recognition motif provided by the adjacent Idu moieties may facilitate docking to the virus. The heparin conformations selected allow two sulfate groups from both GlcN-2 and GlcN-4 to interact with the same ligand, Arg56 of VP3. The r.m.s.d. for all atoms between CONF1 and CONF2 is 1.7 Å. Superposition of the central trisaccharide with the analogous fully sulfated central trisaccharide bound to bFGF (Faham *et al*., 1996) gives an r.m.s.d. of 2.9 Å for CONF1 and 3.1 Å for CONF2. The similarity in the overall disposition of the sugars between the FMDV and bFGF complexes extends to the less well defined outer sugars (as shown in Figure 4B). Of the sulfates that form the key interactions in FMDV, that of GlcN-2 is in a similar relative position in bFGF whereas that of GlcN-4 is radically different (Figure 4B). Thus, significant conformational differences within the sugar rings allow the oligosaccharide to adapt to the markedly different binding sites of FMDV and bFGF whilst maintaining a similar overall shape.

The receptor attachment site

Heparin is bound centrally to the biological protomer of FMDV O_1BFS (Figure 5) within a slight depression of positive electrostatic charge (Figure 6) and makes contacts with all three major capsid proteins (Figure 5D and E). The three sides of the depression (Figure 5C) are formed by (i) strand B1 of VP3 (residues 55–58) and the subsequent loop (residues 58–60, analogous to the 'knob' which forms the south side of the canyon in HRV14; Rossmann *et al*., 1985), (ii) the C-termini of VP1, residues 195–197, and (iii) the αB helix of VP2 (residues 134–138), running perpendicular to the sugar. The base of the depression is formed by a 3_{10} helix (residues 84–87 of VP3) running in the same direction as the sugar. This helix is homologous to helix αA_0 of Mengo virus VP3 which forms part of the putative receptor-binding site (Luo *et al*., 1987). The sequence 200-RHKQI-205 near the C-termini of VP1, previously noted for its similarity to a region of the heparin-binding site of vitronectin (KKQRF) (Fox *et al*., 1989; Kost *et al*., 1992; Jackson *et al*., 1996), does not appear to be involved directly in binding.

The heparin makes ionic interactions with the protein using two sulfates, GlcN-2-2-*N*-SO_3 and GlcN-4-6-*O*-SO_3. These sulfates are 7.7 Å apart and are less mobile than those exposed to the solvent. That they make a substantial contribution to the affinity of the heparin is suggested by the observation that sulfate ions are bound at similar positions in the unliganded virus crystallized from 0.8 M ammonium sulfate (Acharya *et al*., 1989). The 2-*N*-sulfate of GlcN-2 is particularly well matched (Figure 5D). It is interesting that the corresponding binding site is similarly occupied in crystallized unliganded FGF. Arg56 of VP3 plays a central role in organizing the sulfate groups, making interactions with both. The use in this way of the fixed geometry of the guanidinium group may be a mechanism for conferring specificity despite the inherent flexibility of the side chain. The role of this residue was investigated by crystal soaking experiments (at 3 mM) with a closely related O_1 isolate, O_1Kcar2, which differs from O_1BFS in just six residues (Lea *et al*., 1995), including a histidine in place of the arginine at residue 56 of VP3 (Figure 6). No evidence of bound heparin was seen in these crystals, nor could binding by this virus to HS be detected by enzyme-linked immunosorbent assay (ELISA) using paraformaldehyde-fixed BHK or RS2 cells (Figure 6). These results clearly confirm that histidine at VP3 56 drastically reduces the affinity of O_1 FMDV for heparin and HS. In contrast, O_1KB64, which possesses an arginine at position 56 of VP3, is a strong HS binder (Figure 3; see also Jackson *et al*., 1996).

A further arginine residue, Arg135 of VP2, plays a subsidiary role in heparin binding by interacting via bridging water molecules with GlcN-4 and Idu-5 in CONF2, and also probably polarizes Asn88 of VP3, increasing its affinity for GlcN-46-*O*-SO_3. There do not appear to be any protein interactions with Idu-5 in CONF1 and there are no interactions with Idu-1 in either CONF1 or CONF2. That the sugar, at a concentration of ~3 mM, fully displaces the sulfates (present at a concentration of 0.8 M) suggests that the interaction with the sugar is not purely ionic (although entropy and avidity may also favour the binding of the larger molecule). Non-ionic features include the interactions between His195 of VP1 and the central Idu ring, including a van der Waals stacking interaction (~5 Å separation) between the apolar patch of GlcN-4 and the imidazole ring of the histidine (which rotates by 36° about C_β to fulfil this role). Although there does not appear to be a similar stacking interaction in the FGF–heparin complex, such interactions have been observed frequently in monosaccharide complexes such as sucrose with lentil lectin (Casset *et al*., 1995). The ligands are residues 134, 135 and 138 of VP2, residues 56, 59, 60, 87 and 88 of VP3, and residue 195 of VP1 (Figure 5D and E), with bridging water molecules playing an important part. There are virtually no conformational changes in the protein to accommodate the sugar, except for the side chain of His195 of VP1 (in which mobility previously has been noted; Lea *et al*., 1995). Nevertheless, beyond residue 195, the C-terminus of VP1 becomes better ordered (average *B*-factor of 42 Å^2 in the native virus and 34 Å^2 in the complex, whereas the overall mean *B*-factors for the main chain atoms of the proteins are 16 Å^2 in both cases). It is possible that the C-terminal residues of VP1 may stabilize His195 in a position suitable for heparin binding. This would explain the reduction in cell binding for serotypes O_1BFS and A10 when the C-terminal residues are cleaved by trypsin (Fox *et al*., 1989).

Relationship with the integrin-binding site

The RGD integrin recognition motif in the ordered VP1 G–H loop of the reduced virus (Logan *et al*., 1993) is ~15 Å from the closest sugar moiety, Idu-5 (Figure 5A), and our structural data demonstrate that it is unaffected by heparin binding. Electron density maps calculated at lower resolution (4 Å) (to filter out high frequency noise

which might mask a weak signal from a disordered part of the structure) were calculated for the more disordered oxidized state (i.e. crystallized without DTT), which showed no differences compared with the non-bound structure (although with the latest phases we see traces of density for the loop). The two binding sites therefore

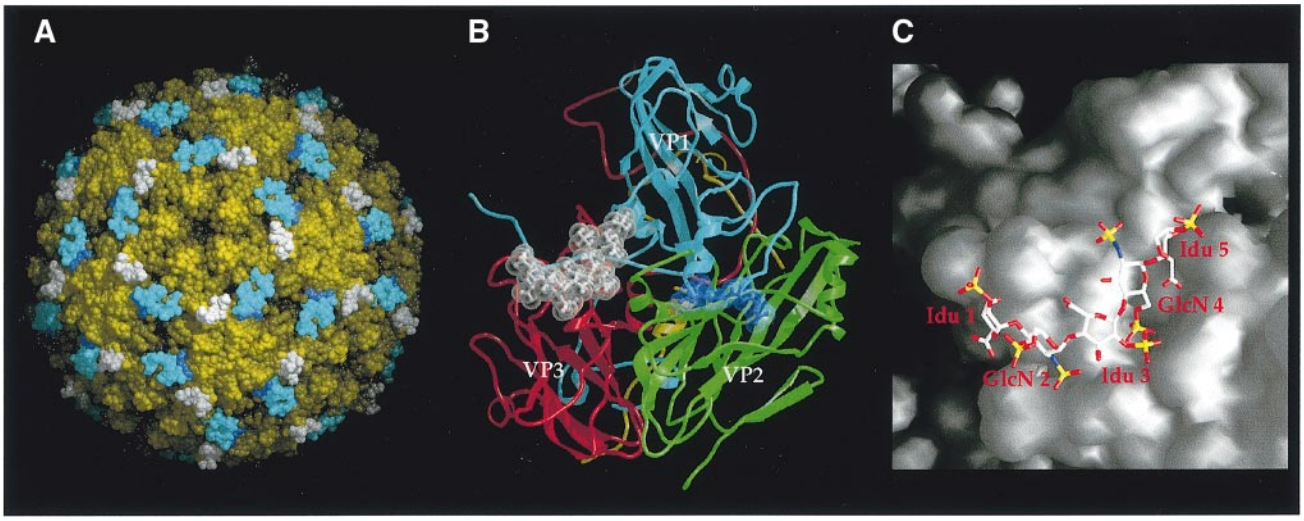

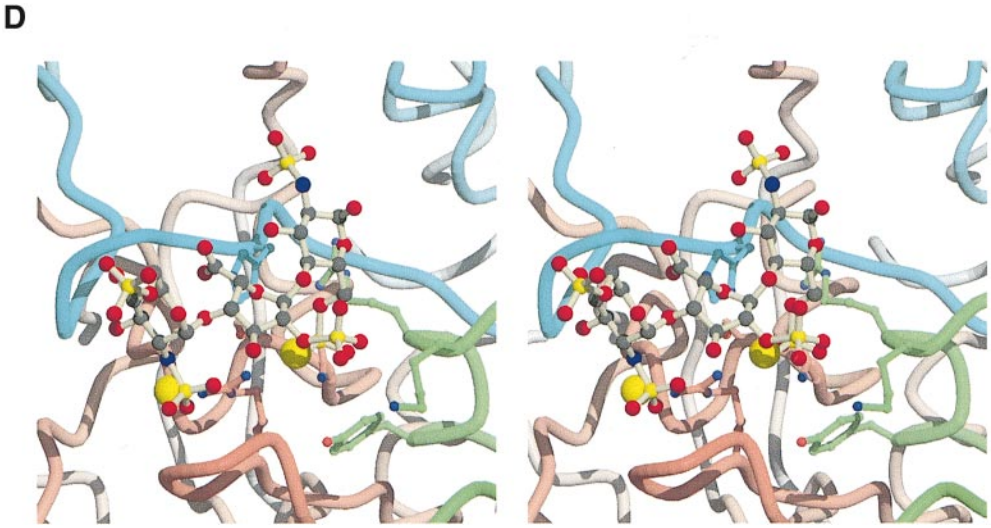

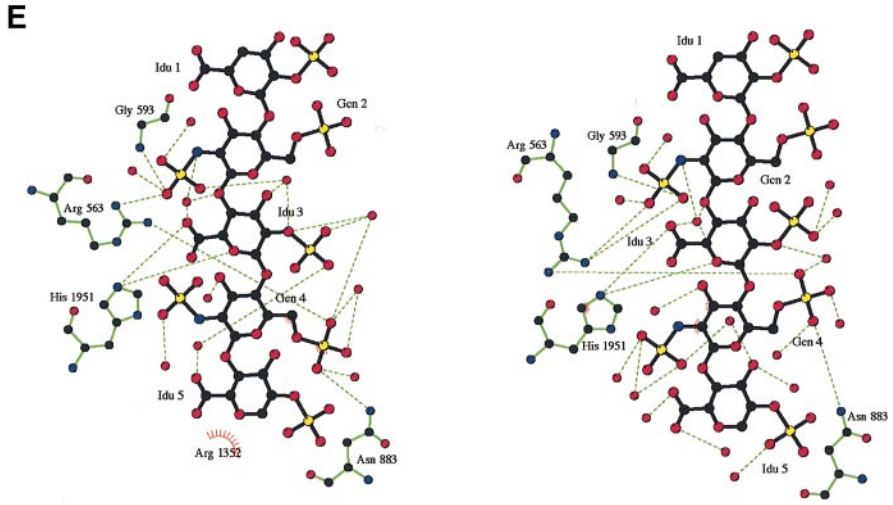

appear independent; nevertheless, we would expect that the very bulky integrin heterodimer would compete with HS binding at the adjacent sites.

Discussion

Basis of receptor specificity and affinity

The relatively large pores extending through the virus crystals have permitted us to visualize an FMDV–GAG receptor complex by soaking. The GAG binds in a groove (Figure 5C) in the centre of the biological protomer constructed from structural components analogous to those that form the so-called 'pit' in Mengo virus (Luo *et al*., 1987) (Figure 5D). The binding site recognizes the fully sulfated form of heparin, as does bFGF (Faham *et al*., 1996). For FMDV, the minimal or tightest binding sequence appears to be a trisaccharide, as found for the complex of polyomavirus with sialic acid (Stehle *et al*., 1994) and of bFGF with HS (Faham *et al*., 1996). Whilst the HS motifs recognized by bFGF and FMDV are in a similar conformation, selectivity is achieved differently. In FMDV, there are hydrogen bonds to the carboxyl and ring oxygen of the Idu, and to the sulfate groups of the GlcN rings (a 6-*O*-sulfate and 2-*N*-sulfate), whilst in bFGF, the interactions are with two *N*-linked GlcN sulfates and the *O*-linked Idu sulfate. Arg56 of VP3 is crucial to the interaction with FMDV, and bridging waters appear to be important in stabilizing the FMDV complex. The FMDV heparin-binding site is recessed [akin to the sialic acid-binding groove in polyoma virus (Stehle and Harrison, 1996) and influenza hemagglutinin (Weis *et al*., 1988)], suggesting that shape complementarity contributes to receptor specificity. Indeed the protein conformation remains essentially unchanged; however, conformational flexibility of the Idu ring (Casu *et al*., 1988) may facilitate binding.

A single point of attachment is unlikely to be sufficient to explain the observed affinity of 10^{-9} M for FMDV bound to fixed cell HS (Jackson *et al*., 1996) since the central trisaccharide occludes only ~280 Å^2 of solvent-accessible surface on the virus and is heavily dependent on a single amino acid for affinity. HS chains contain discrete patches, each comprising 4–8 heavily sulfated sugars suitable for binding virus, separated by ~50 Å (J.Gallagher, personal communication). This spacing approximately matches the distance (a little less than 70 Å) between neighbouring HS attachment sites on the virus (Figure 5A). The high affinity is probably achieved by the flexible sugar chain wrapping around the virus, taking in several binding sites on the virus particle or even multiple particles, as suggested by the inhibition data of Figure 3B, which shows clear evidence of virus cross-linking by heparin.

Receptor adaptation: a driving force in virus evolution?

In subtype O_1 viruses, Arg56 of VP3 confers high affinity HS binding on O_1BFS and O_1KB64, which require HS to infect CHO cells efficiently. These two strains were both adapted to growth in BHK-21 cells (O_1KB64 was passaged 64 times), whereas the HS-independent O_1Kcar2, although from the same cattle outbreak as O_1KB64, was produced with minimal exposure to BHK cell culture (Xie *et al*., 1987). We have determined the coat protein sequences of 20 independent O_1 FMDVs isolated from outbreaks over the past 25 years without recourse to passage in BHK-21 or other established cell lines. Every one has a histidine at VP3 56 (data not shown), confirming that the H56R substitution in VP3 is an adaptation to cell culture, which agrees with the data of Sa-Carvalho *et al*. (1997) and Neff *et al*. (1998).

The dominant hypothesis, until now, has been that the receptor 'footprint' on the capsid surface will be conserved whilst antigenic variation occurs at other surface residues (Rossmann *et al*., 1985). This does not fit with our observations; thus the HS and integrin receptor attachment sites, between them, overlap three of the five antigenic sites of FMDV. Furthermore, some residues central to the antigenic sites are also key points of attachment to the receptors, notably Arg56 of VP3 (Figure 7). Many viral receptors belong to families of related cell surface molecules, so that receptor switching may be relatively facile and indeed has been reported recently for HIV (Wu *et al*., 1996), Theiler's virus (Jarousse *et al*., 1994, 1996; Zhou *et al*., 1997) and polyoma virus (Stehle *et al*., 1994; Stehle and Harrison, 1996). Although there is no evidence for positive Darwinian selection on the bulk of the accessible surface of FMDV (Haydon *et al*., 1998), we suggest that at key points on the virus surface there is interplay between receptor selection and antigenic variation. In this situation, the host defences might provide a motor for receptor switching by selection of a virus with an alternative receptor.

Fig. 5. (**A**) A space-filling representation of the reduced O_1BFS virus (structure determined in the presence of DTT). The surface is shaded according to radius using Bobscript (Esnouf, 1997) and RASTER3D (Merritt and Murphy, 1994). The FMDV VP1 G–H loop (residues 134–157) is highlighted in cyan, with the RGD integrin-binding tripeptide (residues 145–147) picked out in a brighter blue. The heparin motif is shown in white. The distance from one heparin attachment site to both its 5-fold neighbour and its 3-fold neighbour is a little less than 70 Å, whilst the nearest 2-fold-related neighbour is ~90 Å away. (**B**) Ribbon cartoon of the reduced O_1BFS biological protomer with proteins colour coded as in Figure 1. The heparin coordinates for five sugars (CONF1), running left to right, are shown in white ball-and-stick and transparent CPK representation. The RGD integrin-binding motif is highlighted in blue ball-and-stick and transparent CPK representation. (**C**) A Grasp (Nicholls *et al*., 1991) accessible surface representation (grey) showing the binding depression occupied by the five sugar rings with bonds drawn as rods and coloured using the standard convention. (**D**) A ball-and-stick representation of the central three heparin sugars (with conventional atom colours). The protein backbones are drawn with the colouring scheme defined in Figure 1; side chains interacting with the heparin are in ball-and-stick and coloured as the protein backbone; His195 of VP1, Lys134, Arg135 and Tyr138 of VP2, and Arg56, Ser87 and Asn88 of VP3. Bridging water molecules have been excluded for clarity. Yellow spheres mark the positions at which sulfates bind in the native virus. (**E**) Sugar–protein interactions depicted using LIGPLOT (Wallace *et al*., 1995) for each of the bound conformations, CONF1 (left) and CONF2 (right). Note that only the protein side chains that interact directly are shown and that these are rearranged to clarify the hydrogen-bonding pattern. They are labelled with the residue number and the chain ID as the least significant digit, e.g. 563 is residue 56 of VP3. Ligand bonds are drawn in black and non-ligand bonds in green. Hydrogen bonds are depicted by olive green dashed lines. Non-ligand residues involved in hydrophobic contacts are shown as a red, fringed semi-circle. Water molecules are coloured red.

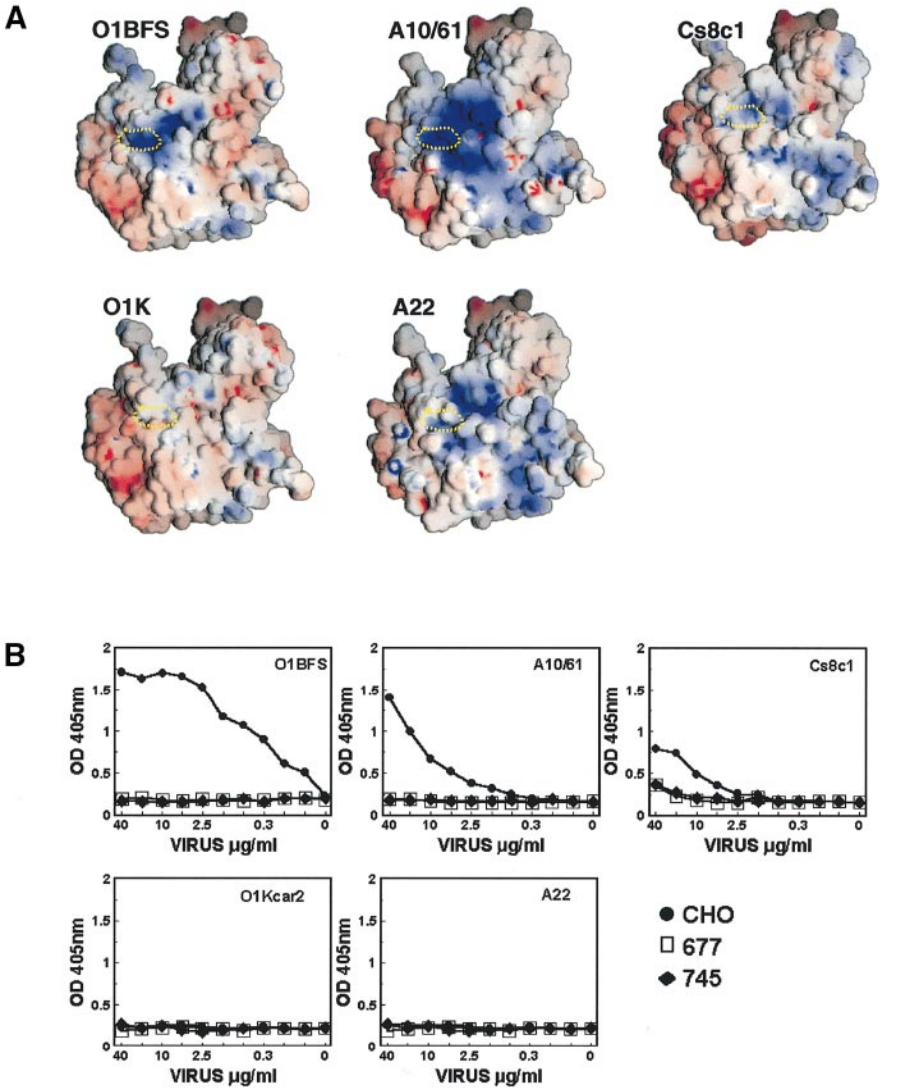

C

Residue number	VP 2 134	VP2 135	VP2 138	VP3 56	VP3 59	VP3 60	VP3 87	VP3 88	VP1 195	Passage history
FMDV										
A10/61	t	r	y	**r**	d	g	s	n	k	H
A22	p	r	y	**c**	e	g	s	n	e	19
Cs8c1	d	r	y	**m**	-	n	s	n	q	L
O1BFS	**k**	**r**	**y**	**r**	**g**	**g**	**s**	**n**	**h**	**H**
O1Kcar2	k	r	y	**h**	g	d	s	n	h	6

Fig. 6. (**A**) Grasp (Nicholls *et al*., 1991) electrostatic, accessible surface representations for the biological protomer of FMDVs for which three-dimensional structures have been determined; O_1BFS, O_1Kcar2, A22, Cs8c1 (Acharya *et al*., 1989; Lea *et al*., 1994, 1995; Curry *et al*., 1996), A10/61 (E.E.Fry, S.Curry, J.W.I.Newman, T.Jackson, W.E.Blakemore, S.M.Lea, A.M.Q.King and D.I.Stuart, unpublished results). Note that the VP1 G–H loop is absent in all these representations. The scale on which the electrostatic potential was coloured was similar for each subtype, with positive charge in blue and negative in red. The position of the heparin-binding site in O_1BFS is delineated in yellow and shown approximately on the other structures. (**B**) A comparison of virus binding to fixed CHO and GAG mutant cells carried out as described in Materials and methods. Binding of FMDV strains O_1BFS, A10/61 and CS8c1 was significantly higher to CHO than to the GAG mutant cells (677 and 745). Virus binding for strains O_1Kcar2 and A22 was virtually identical for all three cell lines and was never greater than background. Each point on the graph represents the mean of duplicate wells. (**C**) A structural-based sequence alignment of the O_1BFS heparin ligands in other aphthoviruses for which the three-dimensional structure is known. The row highlighted corresponds to the serotype in the complex reported here. The column highlighted is the key ligand. The passage history refers to the number of passes in BHK cells (H = highly passaged, L = low passage number). It should be noted that all these viruses were processed for crystal growing and were thus plaque purified. From initial plaquing to crystals requires a minimum of six passes in BHK cells.

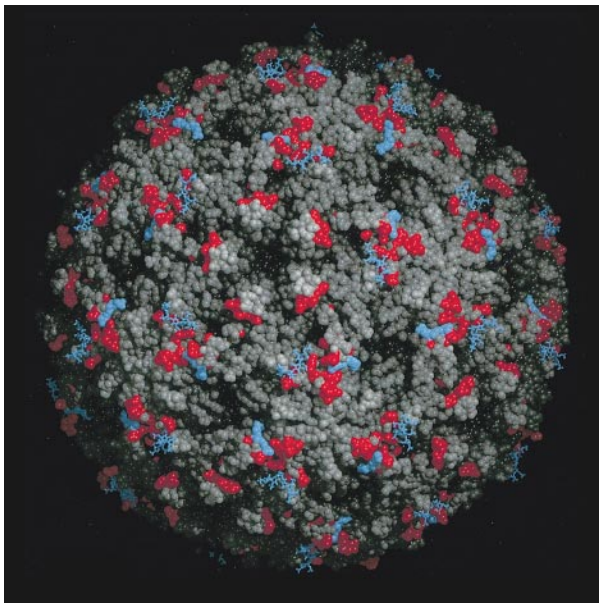

Fig. 7. A space-filling representation of the reduced O_1BFS virus surface shaded according to distance from the particle centre using Bobscript (Esnouf, 1997) and RASTER3D (Merritt and Murphy, 1994). Amino acid substitutions identified at antigenic sites of type O FMDV (Kitson *et al*., 1990; Crowther *et al*., 1993) are shown in red. The integrin-binding RGD is highlighted in pale blue, as is the bound heparin, which is depicted using ball-and-stick representation.

Possible mechanisms of HS-mediated cell entry

O_1BFS virus is almost completely dependent on HS for the ability both to bind to and infect CHO cells, suggesting that increased binding somehow enhances susceptibility; but how? HS might function as an accessory molecule, as it does for several herpes viruses (Spear, 1993), enhancing the efficiency of a second, internalization, receptor. The affinity of O_1BFS for HS is considerably less than for integrins [either in the form of immobilized $\alpha_v\beta_3$ (Jackson *et al*., 1997) or as found on fixed MDBK cells (Figure 3A)], facilitating transfer of the virus from the HS to the integrin. An abundant surface molecule like HS might accelerate virus uptake by concentrating the virus at the cell surface, thereby improving its chance of encountering a slower binding integrin receptor. This mechanism of enhancing the infection rate would not require especially tight binding. A crude calculation suggests that, at a density of $\sim 5\times10^6$ sites/cell (Figure 3A), a receptor would operate with an effective concentration at the cell surface of $\sim10^{-4}$ M, enough to concentrate even a weakly binding virus, especially since a virion can bind multiple proteoglycan receptors.

Virus uptake may be accelerated further through direct interactions between proteoglycan and integrin receptors. Several adhesion molecules, including vitronectin and fibronectin, share with FMDV a dual affinity for integrin and HS (Felding-Harbermann and Cheresh, 1993; Potts and Campbell, 1994), and it is likely that the two types of receptor are capable of interacting with each other to facilitate ligand transfer between them and/or as a mechanism of integrin activation. Whilst we did not observe any conformational change in the integrin-binding loop of the virus on binding heparin, this does not preclude the possibility of integrins and HS proteoglycans interacting with each when bound close together on the virus surface; indeed some contact between such bulky ligands would be almost unavoidable. Recent studies of fibronectin have shown HS- and integrin-binding sites close in space but on opposed molecular faces, suggesting that the two receptors may bind simultaneously (A.Sharma, personal communication).

For high affinity strains like O_1BFS, there are several reasons for thinking that HS proteoglycans may be able, by themselves, to internalize FMDV, without the mediation of integrins. Mason *et al.* (1994) have shown that integrin receptors can be bypassed readily by binding FMDV to an alternative (in their case, Fc) receptor, and Neff *et al*. (1998) have shown that O_1BFS can replicate in human cells that do not express $\alpha_v\beta_3$. Secondly, some membrane proteoglycans undergo endosomal cycling (Yanagishta and Hascall, 1984; Iozzo, 1987) and, therefore, are potential internalizing receptors. Thirdly, multiple passage in cell culture was found recently to select a variant type C FMDV which, when exposed to antibody against the integrin-binding loop, became able to dispense with its RGD motif (Martinez *et al*., 1997), implying that it had acquired an increased affinity for an alternative receptor, such as HS.

GAG receptors in the infected animal

If strong HS binding by FMDV is an adaptation to tissue culture, what role do GAGs play as FMDV receptors in nature? Preliminary measurements of HS-specific binding to paraformaldehyde-fixed CHO cells reveal a wide spectrum of affinities among the seven FMDV serotypes, demonstrating that a predisposition for binding HS is not confined to members of the O_1 subtype (Figure 6B). Given the variability in HS contact residues (Figure 6C), it is not immediately clear if there is an underlying structural conservation in the different GAG-binding sites, or if each site was created *de novo*. This question, which has wide implications for the way proteins in general evolve polysaccharide-binding sites, has not been answered definitively. However, several lines of evidence suggest that FMDVs possess a structurally conserved depression which is predisposed to acquire by mutation a high affinity for HS, the site being positively charged in the high affinity state and observed in all strains of the serotypes (O, A and C) solved to date (Figure 6A).

The difference between fixed and live cells and the evidence for oligovalent interactions with soluble forms of HS indicate that effective receptor density is a key determinant of binding. This enables us to make predictions about the role of this site in field strains, although whether field strains have even a low affinity for HS remains to be established. Selective forces in cell culture are likely to be very different from those in the animal; thus, strains not passaged extensively in BHK cells (where selection is for tight binding rather than for a balance of binding and effective spread) all have VP3 His56, rather than arginine (which confers high affinity and presumably poor spread). Similarly for two other viruses that interact with oligosaccharide receptors on the cell surface, influenza virus and polyoma virus, full virulence requires either limited receptor affinity (Stehle and Harrison, 1996) or a reduction in their number through the action of the viral neuraminidase (Palese *et al*., 1974; Gubareva *et al*., 1995).

Table II. Model refinement statistics

Range of Bragg spacings	12.0–1.9 Å		
Total no. of reflections used	480 760		
Total non-hydrogen protein atoms	5908		
Sugar atoms (summed over two conformations)	170		
Solvent molecules	647		
R_{model} (all data)[a]	16.2 %		
	Protein	Sugar (CONF1)	Sugar (CONF2)
R.m.s.d. bond length[b]	0.014 Å	0.007 Å	0.006 Å
R.m.s.d. bond angles[c]	1.9°	0.97°	1.89°
R.m.s.d. *B* (bonded)[d]	3.6 Å^2	4.58 Å^2	5.39 Å^2
R.m.s.d. *B* (angle-related)[e]	5.6 Å^2	7.69 Å^2	8.87 Å^2

[a] $R_{model} = \frac{\sum_h |(|F_{h,obs}| - |F_{h,calc}|)|}{\sum_h F_{h,obs}|} * 100$

[b]Root mean square deviation from ideal covalent bond lengths.
[c]Root mean square deviation from ideal covalent bond angles.
[d]Root mean square deviation of *B*-factors for the bond restraints.
[e]Root mean square deviation of *B*-factors for the angle restraints.
A total of 90.2% of residues lie in the most favoured region of the Ramachandran plot (Laskowski *et al*., 1993).

For polyoma, selection in the wild is for moderate to tight binders since weak binders are so virulent (Freund *et al*., 1991; Bauer *et al*., 1995). It seems that the virulence 'set point' in the wild will vary with the nature of the infection and mechanism of spread. For FMDV, one possibility discussed earlier is that weak binding to HS proteoglycans serves to increase the rate of integrin-mediated virus uptake. Alternatively, the site may be specific for some other, as yet unidentified, ligand in the natural host, presumably structurally related to HS, and involved in cell entry. It should also be considered that the potential to be a strong GAG binder is itself selectively advantageous. In the infected animal, the virus might routinely switch into, and out of HS-binding mode to pervade particular tissues and, commensurate with the reduced virulence observed (Neff *et al*., 1998), may provide a mechanism of persistent infection—a longstanding puzzle to virologists.

Materials and methods

Cells and viruses

Cells were cultured as described (Jackson *et al*., 1996). Preparation of virus stocks and ^{35}S labelling and purification on sucrose gradients of FMDV strain O_1KB64 have been described (Jackson *et al*., 1997). The specific activity of radiolabelled virus was estimated by ELISA, standardized against purified unlabelled virus assuming an E260 nm of 10.0 for a 1 mg/ml solution.

Infectious centre assay

Confluent cell monolayers (CHO and pgsA-677) were infected at 37°C with O_1BFS at a multiplicity of infection of 0.5 p.f.u./cell. Virus titres in p.f.u./ml were determined on wild-type CHO cells. At the indicated times post-infection, cells were washed with phosphate-buffered saline (PBS) pH 5.0 for 2 min, removed from the dish with trypsin (2 min at 37°C), collected by centrifugation and given a further wash in acid PBS for 2 min. The final cell pellet was resuspended in 500 µl of PBS pH 7.5. A log dilution series of the cells in PBS was layered onto subconfluent BHK cell monolayers in an infectious centre assay as described (Jackson *et al*., 1996). The zero time point was determined using parallel cell monolayers that were exposed to virus for 15 min at 4°C and then treated as above.

Cell-binding studies

Binding experiments were done with purified ^{35}S-labelled FMDV O_1KB64. For experiments with live cells, cell monolayers in 24-well plates were pre-cooled to 4°C, washed with cold PBS pH 7.5 and non-specific binding sites blocked at 4°C for 60 min with BBB [20 mM HEPES pH 7.4, 150 mM NaCl, 1 mM $CaCl_2$, 1 mM $MgCl_2$, 1 mM $MnCl_2$, 1% bovine serum albumin (BSA)], and incubated with 150 µl of virus in BBB at 4°C. The supernatant was removed, and the cell sheet washed twice with PBS. Bound virus was measured by resuspending the cell fraction in 0.25 ml of 0.5% SDS, and mixing, together with 2×0.25 ml H_2O washings, with 1.5 ml of Optiscint liquid scintillant for radioactivity estimation. For Scatchard analyses (Figure 3A), radioactivity in the unbound virus was also measured by counting the pooled supernatant fractions in the same way. Binding to paraformaldehyde-fixed cells was determined by incubating cell monolayers in 96-well plates with 50 µl of virus solution at room temperature for 3 h. Bound and unbound fractions were separated and counted as above, except that the former were solubilized by treatment with 2×100 µl of 2 M NaOH at 80°C for 10 min.

Binding of viruses to GAG mutant cells

Wild-type CHO cells and the GAG-deficient mutant CHO cell lines (677 and 745) were cultured as described (Jackson *et al*., 1996). The line 677 is deficient in HS but makes a greater amount of chondroitin sulfate than CHO cells, whereas 745 cells make little if any GAG (Esko *et al*., 1987). Binding of viruses to paraformaldehyde-fixed cells was carried out as described (Jackson *et al*., 1996) (Figure 6B). Briefly, cell monolayers in 96-well plates were fixed with paraformaldehyde, extensively washed and blocked sequentially with 0.1 M glycine pH 7.2 and BSA in HEPES-buffered saline. Virus was bound to paraformaldehyde-fixed cells for 45 min at room temperature. Unbound virus was removed by washing and bound virus detected using serotype-specific polyclonal rabbit or guinea pig antisera followed by an anti-immunoglobulin alkaline phosphatase conjugate.

X-ray crystallographic analyses

Crystals of FMDV O_1BFS (space group I23, a = 345 Å) were grown using ammonium sulfate as precipitant (Fox *et al*., 1987). Crystals were soaked in 3 kDa/6 kDa heparin or HS (in the form of a sodium salt from Sigma) at a concentration of 20 mg/ml, pH 7.5 for at least 4 h prior to mounting in quartz capillaries. For some crystals, the mother liquor was exchanged for 30% PEG 4K prior to soaking and other crystals were treated with DTT (Logan *et al*., 1993) to permit ordering of the integrin receptor attachment site (the VP1 G–H loop). Crystals of O_1K also grown from ammonium sulfate (Curry *et al*., 1992) were soaked with 20 mg/ml 6 kDa heparin. Diffraction images were collected as 0.3° or 0.5° oscillations, at room temperature on a 30 cm MARRESEARCH imaging plate at the Central Laboratory of the

Research Councils (CLRC), Daresbury Laboratory, Synchrotron Radiation Source (SRS), station 9.6, λ = 0.87Å. Intensities were measured and merged using the DENZO and SCALEPACK programs (Otwinoski, 1993) and converted to structure factor amplitudes using TRUNCATE (French and Wilson, 1978) (Table I presents a summary of the data collected). Difference $[F_{o(soak)} - F_{o(nat)}]$ and $[F_{o(soakA)} - F_{o(sokB)}]$ electron density maps were calculated with phases for the native virus and 5-fold averaged using GAP (J.M.Grimes and D.I.Stuart, unpublished). A model of heparin (courtesy of D.Rees; Faham *et al*., 1996) was fitted to the density at 2.5 Å and modified using FRODO (Jones, 1985). Minor alterations were made to a few protein side chains in the vicinity of the sugar, and more water molecules were incorporated. Unaveraged maps were checked for differences in conformation between the five copies in the crystallographic asymmetric unit. Difference maps between the various sugar soaks were checked for indications of different sugar ring substituents or conformations. Iterative positional and *B*-factor refinement (XPLOR) (Brünger, 1992) [using appropriate stereochemical parameters for the heparin (Faham *et al*., 1996) and Engh and Huber parameters for the protein (Engh and Huber, 1991) with NCS constraints and a bulk solvent correction (Brünger, 1992)], followed by some simulated annealing refinement, was combined with rebuilding and the calculation of sugar omit maps. Refinement of this model against 1.9 Å data provided clear visual evidence for two distinct conformations. Rebuilding into a 1.9 Å map to take account of these two conformations and further cycles of refinement assuming both sugar conformations to be at half occupancy (Table II) produced the final model. Strict NCS constraints were maintained since unaveraged maps did not show any significant deviation between the sugar in each of the five independent non-crystallographically related subunits. To verify that there were no changes in the less well ordered parts of the structure, low resolution (4 Å) $2F_o - F_c$ and $F_o - F_c$ maps were calculated (F_c being those for the refined model).

Acknowledgements

We thank our disease security officers David Goodridge and Stuart Williams, the staff at the DRAL for help with data collection, John Gallagher for helpful discussions, Richard Bryan, Robert Esnouf and Kathryn Measures for computing, and Stephen Lee for digital imaging. This project was supported by the BBSRC and MAFF. D.I.S. and E.F. are supported by the MRC, and S.L. is the Royal Society Dorothy Hodgkin Fellow. The OCMS is supported by the BBSRC, EPSRC and MRC. Atomic coordinates will be deposited with the Protein Data Bank and are available pre-release from the authors (dave@biop.ox.ac.uk). PDB accession code: 1fhp.

References

Abu-Ghazaleh,R. (1996) Structure and function of the VP1 G–H loop of foot-and-mouth disease virus. PhD Thesis, University of Hertfordshire, UK.

Acharya,R., Fry,E., Stuart,D., Fox,G., Rowlands,D. and Brown,F. (1989) The three-dimensional structure of foot-and-mouth disease virus at 2.9 Å resolution. *Nature*, **337**, 709–716.

Bauer,P.H., Bronson,R.T., Fung,S.C., Freund,R., Stehle,T., Harrison,S.C. and Benjamin,T.L. (1995) Genetic and structural analysis of a virulence determinant in polyomavirus VP1. *J. Virol.*, **69**, 7925–7931.

Baxt,B. and Becker,Y. (1990) The effect of peptides containing the arginine–glycine–aspartic acid sequence on the adsorption of foot-and-mouth disease virus to tissue culture cells. *Virus Genes*, **4**, 73–83.

Berinstein,A., Roivainen,M., Hovi,T., Mason,P.W. and Baxt,B. (1995) Antibodies to the vitronectin receptor (integrin $\alpha_v\beta_3$) inhibit binding and infection of foot-and-mouth disease virus to cultured cells. *J. Virol.*, **69**, 2664–2666.

Brünger,A.T. (1992) *XPLOR Version 3.1*. Yale University Press, New Haven, CT.

Carrillo,E.C., Glachetti,C. and Campos,R.H. (1984) Effect of lysosomotrophic agents on the foot-and-mouth disease virus replication. *Virology*, **135**, 542–545.

Casset,F., Hamelryck,L.R., Brisson,J.-R., Tellier,C., Dao-Thi,M.-H., Wyns,L., Poortmans,F., Pérez,S. and Imberty,A. (1995) NMR, molecular modeling and crystallographic studies of lentil-lectin–sucrose interactions. *J. Biol. Chem.*, **270**, 25619–25628.

Casu,B., Petitou,M., Provasoli,M. and Sinay,P. (1988) Conformational flexibility: a new concept for explaining binding and biological properties of iduronic acid-containing glycosaminoglycans. *Trends Biochem. Sci.*, **13**, 221–225.

Clapham,P.R. and Weiss,R.A. (1997) Spoilt for choice of co-receptors. *Nature*, **388**, 230–231.

Compton,T., Nowlin,D.M. and Cooper,N.R. (1993) Initiation of human cytomegalovirus infection requires initial interaction with cell surface heparan sulphate. *Virology*, **193**, 834–841.

Crowther,J.R., Farias,S., Carpenter,W.C. and Samuel,A.R. (1993) Identification of a fifth neutralizable site on type O foot-and-mouth disease virus following characterisation of single and quintuple monoclonal antibody escape mutants. *J. Gen. Virol.*, **74**, 1547–1553.

Curry,S. *et al*. (1992) Crystallisation and preliminary X-ray analysis of three serotypes of foot-and-mouth disease virus. *J. Mol. Biol.*, **228**, 1263–1268.

Curry,S., Abrams,C.C., Fry,E., Crowther,J.C., Belsham,G.J., Stuart,D.I. and King,A.M.Q. (1995) Viral RNA modulates the acid sensitivity of foot-and-mouth disease virus capsid. *J. Virol.*, **69**, 430–438.

Curry,S. *et al*. (1996) Perturbations in the surface structure of A22 Iraq foot-and-mouth disease virus accompanying coupled changes in host cell specificity and antigenicity. *Structure*, **4**, 135–145.

Engh,R.A. and Huber,R. (1991) Accurate bond and angle parameters for X-ray protein-structure refinement. *Acta Crystallogr.*, **A47**, 392–400.

Esko,J.D., Weinke,J.L., Taylor,W.H., Ekborg,G., Rodess,L., Ananthraramaiah,G. and Gawish,A. (1987) Inhibition of chondroitin and heparan sulfate biosynthesis in Chinese hamster ovary cell mutants defective in galactosyltransferase. *J. Biol. Chem.*, **262**, 12189–12195.

Esnouf,R.M. (1997) An extensively modified version of MolScript which includes greatly enhanced colouring capabilities. *J. Mol. Graph.*, **15**, 132–134.

Faham,J.C., Hileman,R.E., Fromm,J.R., Linhardt,R.J. and Rees,D.C. (1996) Heparin structure and interactions with basic fibroblast growth factor. *Science*, **271**, 1116–1120.

Felding-Harbermann,B. and Cheresh,D.A. (1993) Vitronectin and its receptors. *Curr. Opin. Cell Biol.*, **5**, 864–868.

Feng,Y., Broder,C.C., Kennedy,P.E. and Berger,E.A. (1996) HIV-1 entry cofactor: functional cDNA cloning of a seven-transmembrane, G protein-coupled receptor. *Science*, **272**, 872–877.

Forster,M.J. and Mulloy,B. (1993) Molecular dynamics study of iduronate ring conformation. *Biopolymers*, **33**, 575–588.

Fox,G., Stuart,D., Acharya,K.R., Fry,E., Rowlands,D.J. and Brown,F. (1987) Crystallisation and preliminary X-ray diffraction analysis of foot-and-mouth disease virus. *J. Mol. Biol.*, **196**, 591–597.

Fox,G., Parry,N.R., Barnett,P.V., McGinn,B., Rowlands,D.J. and Brown,F. (1989) Cell attachment site on foot-and-mouth disease virus includes the amino acid sequence RGD (arginine–glycine–aspartic acid). *J. Gen. Virol.*, **70**, 625–637.

French,S. and Wilson,K. (1978) On the treatment of negative intensity observations. *Acta Crystallogr.*, **A34**, 517–525.

Freund,R., Calderone,A., Dawe,C.J. and Benjamin,T.L. (1991) Polyomavirus tumor induction in mice: effects of polymorphisms of VP1 and large T antigen. *J. Virol.*, **65**, 335–341.

Gubareva,L.V., Penn,C.R. and Webster,R.G. (1995) Inhibition of replication of avian influenza viruses by the neuraminidase inhibitor 4-guanidino-2,4-dideoxy-2,3-dehydro-*N*-acetylneuraminic acid. *Virology*, **212**, 323–330.

Haydon,D., Lea,S., Fry,L., Knowles,N., Samuel,A.R., Stuart,D. and Woolhouse,M.E.J. (1998) Characterising sequence variation in the VP1 capsid proteins of foot-and-mouth disease virus (serotype O) with respect to virion structure. *J. Mol. Evol.*, **46**, 465–475.

Iozzo,R.V. (1987) Turnover of heparan sulfate proteoglycan in human carcinoma cells. *J. Biol. Chem.*, **262**, 1888–1900.

Jackson,T., Ellard,F.M., Abu Ghazaleh,R., Brookes,S.M., Blakemore, W.E., Corteyn,A.H., Stuart,D.I., Newman,J.W.I. and King,A.M.Q. (1996) Efficient infection of cells in culture by type O foot-and-mouth disease virus requires binding to cell surface heparan sulfate. *J. Virol.*, **70**, 5282–5287.

Jackson,T., Sharma,A., Abu-Ghazaleh,R., Blakemore,W., Ellard,F., Simmons,D.L., Stuart,D.I., Newman,J.W.I. and King,A.M.Q. (1997) Arginine–glycine–aspartic acid-specific binding by foot-and-mouth disease viruses to the purified integrin $\alpha_v\beta_3$ *in vitro*. *J. Virol.*, **71**, 8357–8361.

Jarousse,N., Grant,R., Hogle,J.M., Zhang,L., Senkowski,A., Roos,R.P., Michiels,T., Brahic,M. and McAllister,A. (1994) A single amino acid change determines persistence of a chimeric Theiler's virus. *J. Virol.*, **68**, 3364–3368.

Jarousse,N., Martinat,C., Syan,S., Brahic,M. and McAllister,A. (1996)

Role of VP2 amino acid 141 in tropism of Theiler's virus within the central nervous system. *J. Virol.*, **70**, 8213–8217.
Jones,T.A. (1985) Interactive computer graphics: FRODO. *Methods Enzymol.*, **115**, 157–171.
Kitson,J.D.A., McCahon,D. and Belsham,G.J. (1990) Sequence analysis of monoclonal antibody resistant mutants of type O foot-and-mouth disease virus: evidence for involvement of the three surface exposed capsid proteins in four antigenic sites. *Virology*, **179**, 26–34.
Kost,C., Stüber,W., Ehrlich,H.J., Pannekoek,H. and Preissner,K.T. (1992) Mapping of binding sites to heparin, plasminogen activator inhibitor-1 and plasminogen to vitronectin's heparin-binding region reveals a novel vitronectin-dependent feedback mechanism for the control of plasmin formation. *J. Biol. Chem.*, **267**, 12095–12105.
Laskowski,R.A., MacArthur,M.W., Moss,D.S. and Thornton,J.M. (1993) PROCHECK: a program to check the stereochemical quality of protein structures. *J. Appl. Crystallogr.*, **26**, 283–291.
Lea,S. *et al*. (1994) The structure and antigenicity of a type C foot-and-mouth disease virus. *Structure*, **2**, 123–139.
Lea,S. *et al*. (1995) Structural comparison of two strains of foot-and-mouth disease virus subtype O1 and a laboratory antigenic variant, G67. *Structure*, **3**, 571–580.
Logan,D. *et al*. (1993) Structure of a major immunogenic site on foot-and-mouth disease virus. *Nature*, **362**, 566–568.
Luo,M. *et al*. (1987) The atomic structure of mengo virus at 3.0 Å resolution. *Science*, **235**, 182–191.
Martinez,M.A., Verdaguer,N., Mateu,M.G. and Domingo,E. (1997) Evolution subverting essentiality: dispensability of the cell attachment Arg–Gly–Asp motif in multiply passaged foot-and-mouth disease virus. *Proc. Natl Acad. Sci. USA*, **94**, 6798–6802.
Mason,P.W., Rieder,E. and Baxt,B. (1994) RGD sequence of foot-and-mouth disease virus is essential for infecting cells via the natural receptor but can be bypassed by an antibody-dependent enhancement pathway. *Proc. Natl Acad. Sci. USA*, **91**, 1932–1936.
Merritt,E.A. and Murphy,M.E.P. (1994) Raster3D version 2.0. A program for photorealistic molecular graphics. *Acta Crystallogr.*, **D50**, 869–873.
Mettenleiter,T.C., Zask,L., Zuckermann,N., Sugg,N., Kern,H. and Ben-Porat,T. (1990) Interaction of glycoprotein gIII with a cellular heparinlike substance mediates adsorption of pseudorabies virus. *J. Virol.*, **64**, 278–286.
Neff,S., Sa-Carvalho,D., Rieder,E., Mason,P.W., Blystone,S.D., Brown,E.J. and Baxt,B. (1998) Foot-and-mouth disease virus virulent for cattle utilizes the integrin $\alpha_v\beta_3$ as its receptor. *J. Virol.*, **72**, 3587–3594.
Nicholls,A., Sharp,K.A. and Honig,B. (1991) Protein folding and association: insights from the interfacial and thermodynamic properties of hydrocarbons. *Proteins*, **11**, 281–296.
Olson,N.H., Kolatkar,P.R., Oliveira,M.A., Cheng,R.H., Greve,J.M., McClelland,A., Baker,T.A. and Rossmann,M.G. (1993) Structure of a human rhinovirus complexed with its receptor molecule. *Proc. Natl Acad. Sci. USA*, **90**, 507–511.
Otwinoski,Z. (1993) Oscillation data reduction program. SERC, Daresbury Laboratory, Warrington, UK.
Palese,P., Tobita,K., Ueda,M. and Compans,R.W. (1974) Characterization of influenza virus temperature sensitive mutants defective in neuraminidase. *Virology*, **61**, 397–410.
Parry,N., Fox,G., Rowlands,D., Brown,F., Fry,E., Acharya,R. and Stuart,D. (1990) Structural and serological evidence for a novel mechanism of immune evasion in foot-and-mouth disease virus. *Nature*, **347**, 569–572.
Potts,J.R. and Campbell,I.D. (1994) Fibronectin structure and assembly. *Curr. Opin. Cell Biol.*, **6**, 648–655.
Rossmann,M.G. *et al*. (1985) Structure of a human common cold virus and functional relationship to other picornaviruses. *Nature*, **317**, 145–153.
Rueckert,R.R. (1996) Picornaviridae: the viruses and their replication. In Fields,B.N. (ed.), *Fields Virology*. Lippincott-Raven Publishers, Philadelphia, PA, Vol. 1, pp. 609–654.
Sa-Carvalho,D., Rieder,E., Baxt,B., Rodarte,R., Tanuri,A. and Mason,P.W. (1997) Tissue culture adaptation of foot-and-mouth disease virus selects viruses that bind to heparin and are attenuated in cattle. *J. Virol.*, **71**, 5115–5123.
Salmivirta,M., Lidholt,K. and Lindahl,U. (1996) Heparan sulfate: a piece of information. *FASEB J.*, **10**, 1270–1279.
Sekiguchi,K., Franke,A.J. and Baxt,B. (1982) Competition for cellular receptor sites among selected aphthoviruses. *Arch. Virol.*, **74**, 53–64.
Spear,P.G. (1993) Entry of alphaherpeviruses into cells. *Virology*, **4**, 167–180.
Stehle,T. and Harrison,S.C. (1996) Crystal structures of murine polyomavirus in complex with straight-chain and branched-chain sialyloligosaccharide receptor fragments. *Structure*, **4**, 183–194.
Stehle,T., Yan,Y., Benjamin,T.L. and Harrison,S.C. (1994) Structure of murine polyomavirus complexed with an oligosaccharide receptor fragment. *Nature*, **369**, 160–163.
Stuart,D.I., Levine,M., Muirhead,H. and Stammers,D.K. (1979) Crystal structure of cat muscle pyruvate kinase at a resolution of 2.6 Å. *J. Mol. Biol.*, **134**, 109–142.
Surovoi,A.Y., Ivanov,V.T., Chepurkin,A.V., Ivanyuschenkov,V.N. and Dryagalin,N.N. (1988) Is the Arg–Gly–Asp sequence the site for foot-and-mouth disease virus binding with cell receptor? *Sov. J. Bioorg. Chem.*, **14**, 965–968.
Wagner,L., Yang,O.O., Garcia-Zepeda,E.A., Ge,Y., Kalams,S.A., Walker,B.D., Pasternack,M.S. and Luster,A.D. (1998) β-Chemokines are released from HIV-1-specific cytolytic T-cell granules complexed to proteoglycans. *Nature*, **391**, 908–911.
Wallace,A.C., Lakowski,R.A. and Thornton,J.M. (1995) LIGPLOT: a program to generate schematic diagrams of protein–ligand interactions. *Protein Eng.*, **8**, 127–134.
Weis,W., Brown,J.H., Cusack,S., Paulson,J.C., Skehel,J.J. and Wiley,D.C. (1988) Structure of the influenza virus haemagglutinin complexed with its receptor, sialic acid. *Nature*, **333**, 426–431.
Wickham,T., Mathias,P., Cheresh,D. and Nemerow,G. (1993) Integrins $\alpha_v\beta_3$ and $\alpha_v\beta_5$ promote adenovirus internalisation but not virus attachment. *Cell*, **73**, 309–319.
Wu,L. *et al*. (1996) CD4-induced interaction of primary HIV-1 gp120 glycoproteins with the chemokine receptor CCR-5. *Nature*, **384**, 179–183.
WuDunn,D. and Spear,P.G. (1989) Initial interaction of herpes simplex virus with cells is binding to heparan sulphate. *J. Virol.*, **63**, 52–58.
Xie,Q.-C., McCahon,D., Crowther,J.R., Belsham,G.J. and McCullough,K.C. (1987) Neutralisation of foot-and-mouth disease virus can be mediated through any of at least three separate antigenic sites. *J. Gen. Virol.*, **68**, 1637–1647.
Yanagishta,M. and Hascall,V.C. (1984) Metabolism of proteoglycans in rat ovarian granulosa cell culture. *J. Biol. Chem.*, **259**, 10270–10283.
Zhou,L., Lin,X., Green,T., Lipton,H.L. and Luo,M. (1997) Role of sialyloligosaccharide binding in Theiler's virus persistence. *J. Virol.*, **71**, 9701–9712.

Received October 2, 1998; revised December 8, 1998; accepted December 9, 1998